Dysregulated Serum Response Factor Triggers Formation of Hepatocellular Carcinoma

Stefan Ohrnberger,[1]* Abhishek Thavamani,[1,2]* Albert Braeuning,[3] Daniel B. Lipka,[2,4] Milen Kirilov,[5] Robert Geffers,[6] Stella E. Authenrieth,[7] Michael Römer,[8] Andreas Zell,[8] Michael Bonin,[9] Michael Schwarz,[3] Günther Schütz,[5] Peter Schirmacher,[10] Christoph Plass,[2,4] Thomas Longerich,[10] and Alfred Nordheim[1,2]

The ubiquitously expressed transcriptional regulator serum response factor (SRF) is controlled by both Ras/MAPK (mitogen-activated protein kinase) and Rho/actin signaling pathways, which are frequently activated in hepatocellular carcinoma (HCC). We generated _SRF-VP16^iHep_ mice, which conditionally express constitutively active SRF-VP16 in hepatocytes, thereby controlling subsets of both Ras/MAPK- and Rho/actin-stimulated target genes. All _SRF-VP16^iHep_ mice develop hyperproliferative liver nodules that progresses to lethal HCC. Some murine (m)HCCs acquire _Ctnnb1_ mutations equivalent to those in human (h)HCC. The resulting transcript signatures mirror those of a distinct subgroup of hHCCs, with shared activation of oncofetal genes including _Igf2,_ correlating with CpG hypomethylation at the imprinted _Igf2/H19_ locus. _Conclusion:_ SRF-VP16^iHep_ mHCC reveal convergent Ras/MAPK and Rho/actin signaling as a highly oncogenic driver mechanism for hepatocarcinogenesis. This suggests simultaneous inhibition of Ras/MAPK and Rho/actin signaling as a treatment strategy in hHCC therapy. (HEPATOLOGY 2015;61:979-989)

Human hepatocellular carcinoma (hHCC) belongs to the five most lethal cancers worldwide.[1] Liver cirrhosis, alcohol abuse, or chronic hepatitis virus infection, and type 2 diabetes-associated nonalcoholic steatohepatitis predispose to HCC. Despite their extreme heterogeneity, hHCCs could be classified (G1-G6, or S1-S3) based on gene expression signatures, genomic and epigenetic alterations.[2-4] Aberrant activation of WNT/β-catenin, Jak/STAT, PI-3K/Akt signaling pathways, and activation of the Ras/MAPK (mitogen-activated protein kinase) and Rho/actin cascades cause HCC formation.[3,5-7] Both Ras/MAPK and Rho/actin cascades regulate cell proliferation and differentiation.[6] Rho/actin signaling additionally determines polarity, adhesion, and mechanosensory and migratory activities of normal and cancerous cells.[8,9] Activation of Rho/actin signaling in hHCC is frequently elicited by deletion of Rho/Rac/Cdc42-inhibiting tumor suppressors, e.g., _DLC1_.[7,8,10] _DLC1_ encodes a Rho inhibitor with Rho-GAP function and is deleted in up to 50% of liver cancers.[7,10] Synergistic oncogenic crosstalk of Ras/MAPK and Rho/actin signaling has been described,[11,12] but their joint impact on target gene expression remains unclear.

The transcription factor SRF (serum response factor) is activated by both Ras/MAPK and Rho/actin signaling, engaging distinct target gene profiles and involving alternative cofactors (ternary complex factors [TCFs], myocardin related transcription factors [MRTFs])[13,14] (Fig. 1A). Elevated expression of SRF was reported in high-grade hHCCs.[15,16] SRF was activated by the X and core proteins of hepatitis B virus (HBV) and C virus (HCV),

respectively.[17] DLC1-deleted HCC cells revealed activation of Rho/actin signaling and associated nuclear localization of SRF cofactors MRTF-A/B (MKL1/2).[18] Furthermore, antiproliferative, prosenescence effects on HCC xenografts were obtained upon down-regulation of MRTFs/MKLs.[19] Collectively, this implies SRF contributions to hHCC formation. We provide here the first *in vivo* evidence supporting this concept. We generated the SRF-VP16^{iHep} mouse line, permitting conditional expression of the SRF-VP16 protein in hepatocytes upon Cre-mediated deletion of a STOP-flox cassette.[20] SRF-VP16 carries the VP16 transcriptional activation domain of *Herpes simplex* virus, thereby eliciting constitutive SRF activity.[21]

In SRF-VP16^{iHep} mice, conditional activation of SRF-VP16 elicited broad changes in hepatocellular gene expression resulting in hyperproliferative nodules, followed by rapid progression to HCC. Importantly, SRF-VP16^{iHep} HCCs share molecular features with distinct subgroups of hHCCs, including overlapping gene expression signatures,[2,22] activating Ctnnb1 mutations,[23] and hypomethylation of Igf2/H19 oncofetal genes.[22] Thus, SRF-VP16^{iHep} mice identify the SRF-mediated convergence of sustained MAPK and Rho/actin signaling as an oncogenic driver of HCC.

Materials and Methods

Stochastic Hepatocyte-Specific Expression of SRF-VP16. Stop-floxed SRF-VP16 mice (Gt(ROSA)26-Sor$^{tm1(SRF-VP16)Antu}$ mice)[20] were bred with Srf-flex1 (floxed Srf exon 1)[24] and Alfp-CreER^{T2} animals (Supporting Fig. 1A) to obtain triple transgenic mice, Srf$^{flex1/wt}$::SRF-VP16$^{+/-}$::Alf-CreER$^{T2+/-}$ (termed SRF-VP16^{iHep}; for polymerase chain reaction [PCR] genotyping: Supporting Materials and Methods). Liver specificity of CreER^{T2} activity (Supporting Fig. 1B), its tamoxifen-inducible activation (Supporting Fig. 1B), and its spontaneous activity (Supporting Fig. 1B,C) are evidenced. Animal housing and handling was in accordance with the Federation of European Laboratory Animal Science Associations and approved by local ethics committees (Regierungspräsidium Tübingen).

The Supporting Materials and Methods describe experimental details for the following: histological analysis, immunoblot analyses, and antibodies for immunoblotting and immunohistochemistry; analysis of genomic mutations of mHCCs; quantitative high-resolution DNA methylation analysis of murine samples; methylation profiling of hHCCs; expression profiling of hHCCs; genomic DLC1 status of hHCCs; CTNNB1 mutational analysis of hHCCs; expression profiling of murine samples; quantitative real-time PCR; isolation and analysis of murine intrahepatic immune cells (IHICs); statistical analysis.

Results

Constitutively Active SRF Causes Liver Expansion in SRF-VP16^{iHep} *Mice.* Mice carrying the conditional Rosa26(SRF-VP16) allele[20] were bred with animals expressing tamoxifen-inducible hepatocyte-specific CreER^{T2} (Alfp-CreER^{T2} mice) (Supporting Fig. 1A,B) to get SRF-VP16^{iHep} mice. Treatment of SRF-VP16^{iHep} mice with tamoxifen caused efficient induction of SRF-VP16 expression. However, marginal spontaneous activity of Cre-recombinase was observed in the absence of tamoxifen, leading to SRF-VP16 expression in a few hepatocytes. Employing the Cre-responsive mT/mG reporter allele (Supporting Materials and Methods), we quantified this spontaneous CreER^{T2} activation to generate per liver, within the first 10 weeks of age, an accumulated total of $0.38\% \pm 0.08\%$ hepatocytes (n = 9) (Supporting Fig. 1C,D).

Spontaneous CreER^{T2} activation in SRF-VP16^{iHep} mice caused hyperproliferation of effected hepatocytes, leading to multiple premalignant nodules throughout the livers, accompanied by age-dependent increases in liver mass reaching a liver weight-to-body weight ratio (LBWR) of up to 33% (Fig. 1C, Supporting Fig. 2). 80% of all animals developed HCC within 25-40 weeks of age (n > 93) (Fig. 1B,C; Supporting Fig. 2). Mice lacking either SRF-VP16 or CreER^{T2} alleles, or both, never developed increased LBWR or HCC during this time (n > 143). In livers of SRF-VP16^{iHep} mice, but not of control animals, recombination and expression of SRF-VP16 was observed at DNA, RNA, and protein levels (Fig. 1D,E).

SRF-VP16^{iHep} livers with LBWR greater than 15% displayed many macroscopically visible premalignant

Fig. 1. Murine hepatocyte-specific expression of SRF-VP16 leads to hepatocarcinogenesis. (A) Ras/MAPK and Rho/actin signaling target the SRF-cofactor module. Constitutively active SRF-VP16 acts independent of upstream signaling. (B) Kaplan-Meier survival curves of *Alfp-CreER*[T2] mice, expressing (red) *SRF-VP16* or not (blue). (C) *SRF-VP16*[iHep] livers show increasing numbers and sizes of premalignant nodules, as well as HCCs (arrowheads), correlating with increasing LBWR (%). (D) *Rosa26(SRF-VP16)* genomic PCR identifies Cre recombination-mediated loss of the STOP-flox cassette (upper). SRF-VP16 RNA expression: qRT-PCR (17 liver samples, increasing LBWR) (lower). (E) Western blotting identifying SRF-VP16 protein. (F) mT/mG-Cre indicator mice reveal spontaneous activation of *Alfp-CreER*[T2] in livers of both control (upper) and *SRF-VP16*[iHep] (lower) mice (10 weeks old), the latter displaying proliferative cell expansion (scale bars = 50 μm).

nodules (Fig. 1C), each likely derived from clonal expansion of an individual SRF-VP16-expressing hepatocyte. In support, we crossed the mT/mG Cre reporter allele into *SRF-VP16*[iHep] mice and identified, at the age of 10 weeks, multiple green nodules representing colonies of hepatocytes with CreER[T2]

activity (Fig. 1F, lower). *Alfp-CreER*[T2] control animals lacking the *SRF-VP16* allele, displayed multiple individual green cells rather than cell colonies (Fig. 1F, upper). Thus, spontaneous CreER[T2]-mediated activation of SRF-VP16 expression in a subset of hepatocytes caused their hyperproliferation, leading
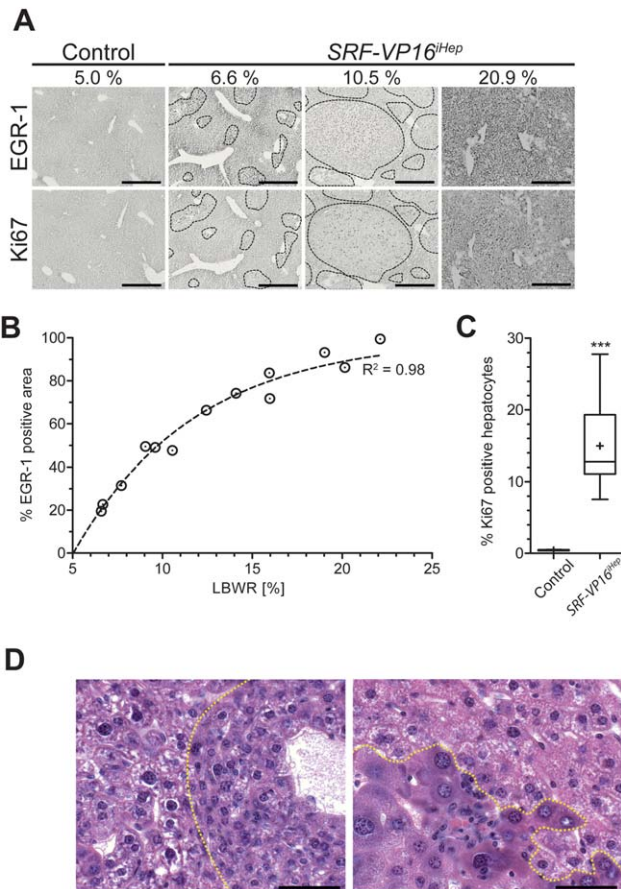
Fig. 2. SRF-VP16 drives hepatocyte hyperproliferation and premalignant nodule formation. (A) Increasing LBWR (%) correlates with expanding premalignant nodules of Egr1-positive (upper) and Ki67-positive (lower) hyperproliferative hepatocytes. Scale bar = 500 μm. (B) Increasing LBWR correlates with sizes (EGR1-positive area) of hyperproliferative nodules (one-phase association: R^2 = 0.977). (C) Quantitation of Ki67-positive hepatocyte nuclei in control (0.4 $\pm$ 0.03%) versus SRF-$VP16^{iHep}$ animals (7.5 to 27.5%; mean 15% $\pm$ 3%) (n = 11). (D) Hematoxylin and eosin (H&E) staining of SRF-$VP16^{iHep}$ livers with LBWR of 7.3% (left) and 10.8% (right). Hyperproliferative nodules display small-cell dysplasia of SRF-VP16 expressing hepatocytes (left panel, right of dotted line). Later stages show severe nuclear atypia, focal inflammatory cell infiltration, and single-cell invasion into the nonneoplastic tissue (right panel, below dotted line). Scale bar = 50 μm.

to premalignant nodules followed by progression to HCC.

Liver Expansion Upon Hyperproliferation of SRF-VP16-Expressing Hepatocytes. Liver histology of SRF-$VP16^{iHep}$ mice revealed foci of small hepatocytes in the perivenular parenchyma indicating hepatocellular proliferation. These foci rapidly expanded to hyperproliferative nodules composed of small basophilic hepatocytes with slightly enlarged nuclei, all strongly expressing the proliferation-associated SRF target gene *Egr1* (Fig. 2A, upper). Increases in nodule size correlated with increasing LBWR (Fig. 2A, upper,

2B). All Egr1-positive nodules showed proliferative activity, displaying an average of 15% Ki67-positive cells (Fig. 2A, lower, 2C). While these nodules initially showed a clear demarcation to surrounding nonneoplastic parenchyma (Fig. 2D, left), in some lesions atypia developed and individual cells infiltrated into the surrounding parenchyma (Fig. 2D, right).

Progression From Hyperproliferative Nodules to HCC. All SRF-$VP16^{iHep}$ livers containing multiple hyperproliferative nodules displayed solid microtrabecular growth of small basophilic hepatocytes (Fig. 3A,A′,D), expressing the polarity marker DPP IV of nontransformed hepatocytes.[25] Above 20 weeks of age, the majority of animals (n = 51) harbored one to several macroscopically visible tumors (Fig. 3A-C) with pseudo-glandular and irregular trabecular growth patterns (Fig. 3E,F) as unequivocal characteristics of HCC. Tumor cells lost expression of DPP IV (Fig. 3E, right). Together, SRF-$VP16^{iHep}$ livers revealed progression from premalignant, hyperproliferative nodules to HCC, as initiated by sporadic hepatocyte-specific expression of SRF-VP16.

Senescent Hepatocytes and Infiltrating Lymphocytes in SRF-VP16^{iHep} Livers. We estimated up to 100,000 hyperproliferative nodules per liver (Figs. 1C, 2A), a high number contrasted with the lower number (less than 5) of HCCs within one liver (Fig. 3A-C). Thus, progression from premalignant nodules to HCC was rare, possibly impaired by cellular tumor-suppressive mechanisms. SRF-$VP16^{iHep}$ livers displayed elevated numbers of β-galactosidase/p21-positive senescent cells (Fig. 4A, upper and middle),[26] unaccompanied by activated caspase 3-mediated apoptotic activity (Fig. 4B). Further, tumor tissue displayed nests of infiltrating immune cells (Fig. 4A), with elevated levels of neutrophils (CD11b^{high}Gr-1$^+$), macrophages (CD11b$^+$F4/80$^+$), and CD8$^+$ T cells, but not CD4$^+$ T cells (Fig. 4C,D).

SRF-VP16-Triggered HCC Progression May Associate With β-Catenin Mutations. In hHCC, activating mutations of the *CTNNB1* are frequently observed.[3] We sequenced the *Ctnnb1* gene of 26 separately dissected SRF-$VP16^{iHep}$ mHCCs. Twelve samples (46%) carried *Ctnnb1* missense mutations affecting codons 32, 34, 37, or 41 (Supporting Table S1), representing frequently mutated codons of *CTNNB1* in human cancers.[23] *Ha-Ras* (codon 61) and *B-Raf* (codon 600) mutations, were not found (not shown).

Expression of Candidate SRF Target Genes. Quantitative real time PCR (qRT-PCR) of candidate gene transcripts from nine control, 17 SRF-$VP16^{iHep}$ nodular
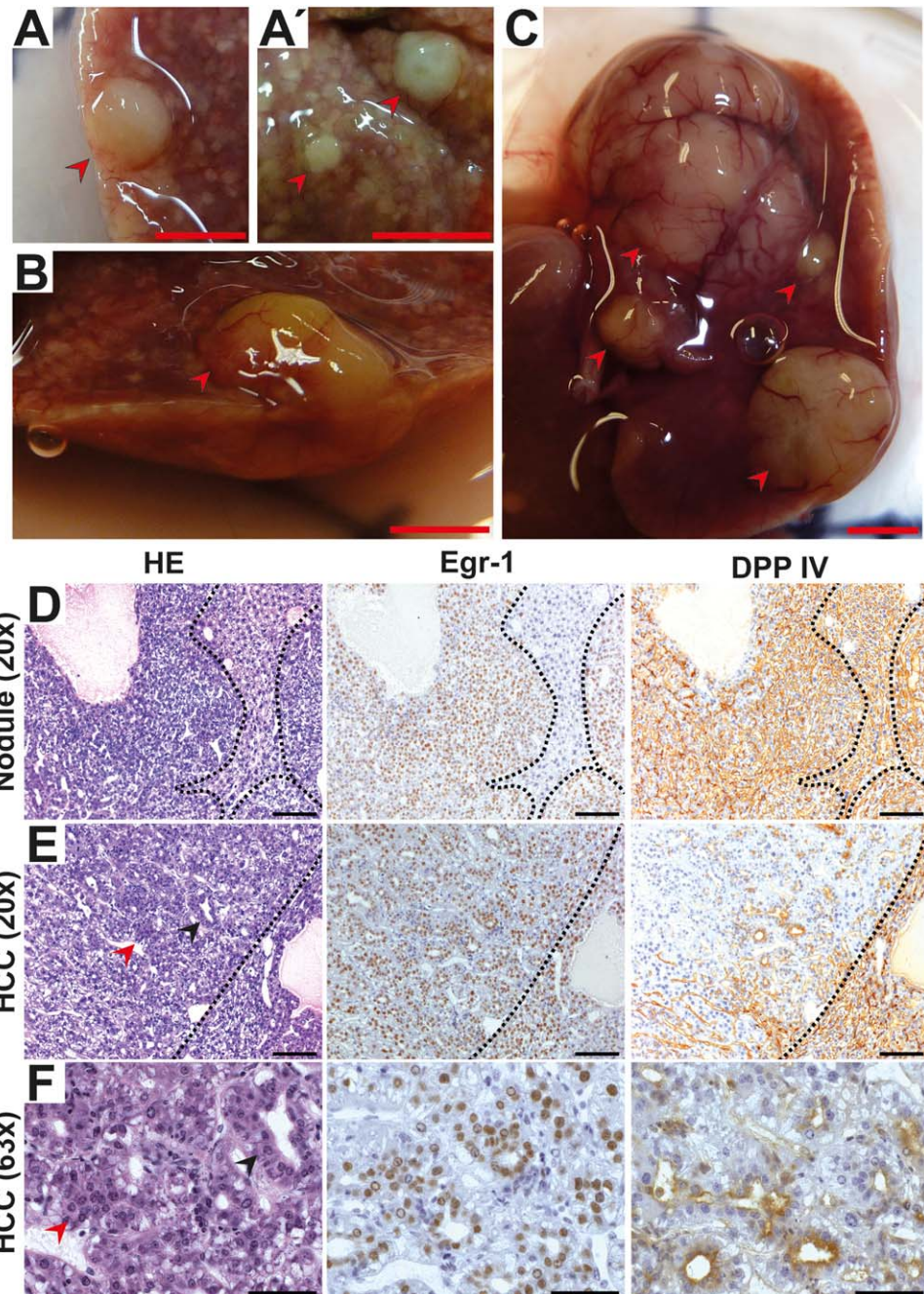
Fig. 3. Malignant transformation to HCC. HCCs of small (0.2-0.5 cm) (A,A′), intermediate (B), or large (>2.5 cm) (C) size. Scale bar = 1 cm. Histology of livers containing premalignant nodules (D) or mHCC tissue (E,F). Scale bars = (D,E) 100 μm, (F) 50 μm. Hyperproliferative nodules are composed of small, basophilic hepatocytes showing a microtrabecular growth (D, left), express the SRF target gene *Egr1* (D, middle), and the polarization marker DPP IV (D, right). HCC tissue characterized by nuclear and architectural atypia in the form of pseudoglandular (black arrowhead) and irregular solid-trabecular growth patterns (red arrowhead) (E, left; F, left). Nuclear Egr1 expression is high throughout the tumor (E, middle; F, middle), residual DPP IV expression is restricted to luminal membranes of pseudoglands (E, right; F, right).

(LBWR, ranging from 6.6 to 26.9%), and five *SRF-VP16^{iHep}* mHCC tissues (Fig. 5) revealed dramatic up-regulation of the proliferation-associated, Ras/MAPK-stimulated immediate-early genes (IEGs) *Egr1*, *Egr2*, and c-*fos* in both nodular and HCC tissue (column (i)). The β-*actin* and *Vinculin* genes, normally regulated by Rho/actin signaling, were also up-regulated in nodular and mHCC tissues (column (ii)). Tumor proliferation genes (*Ctnnb1*, c-*Myc*) were prominently up-regulated in mHCCs (column (iii)). Carcinoma progression genes (*Cdh1*, *Mmp14*, and *Vim*) showed significant up-regulation in nodules and mHCC (column (iv)). Collectively, in *SRF-VP16^{iHep}* mice, liver tissues display up-regulation of direct SRF target genes normally stimulated by either MAPK or Rho/actin signaling.

Genome-Wide Gene Expression Profiling of Murine Tumor Tissues. In genome-wide RNA expression profiling we compared control livers (n = 3) with premalignant nodular liver tissue (n = 3) and HCC tissues carrying either wild-type *Ctnnb1* (mHCC$_A$ tumors) (n = 3) or mutated *Ctnnb1* (mHCC$_B$ tumors) (n = 3). Altogether, about 1,330
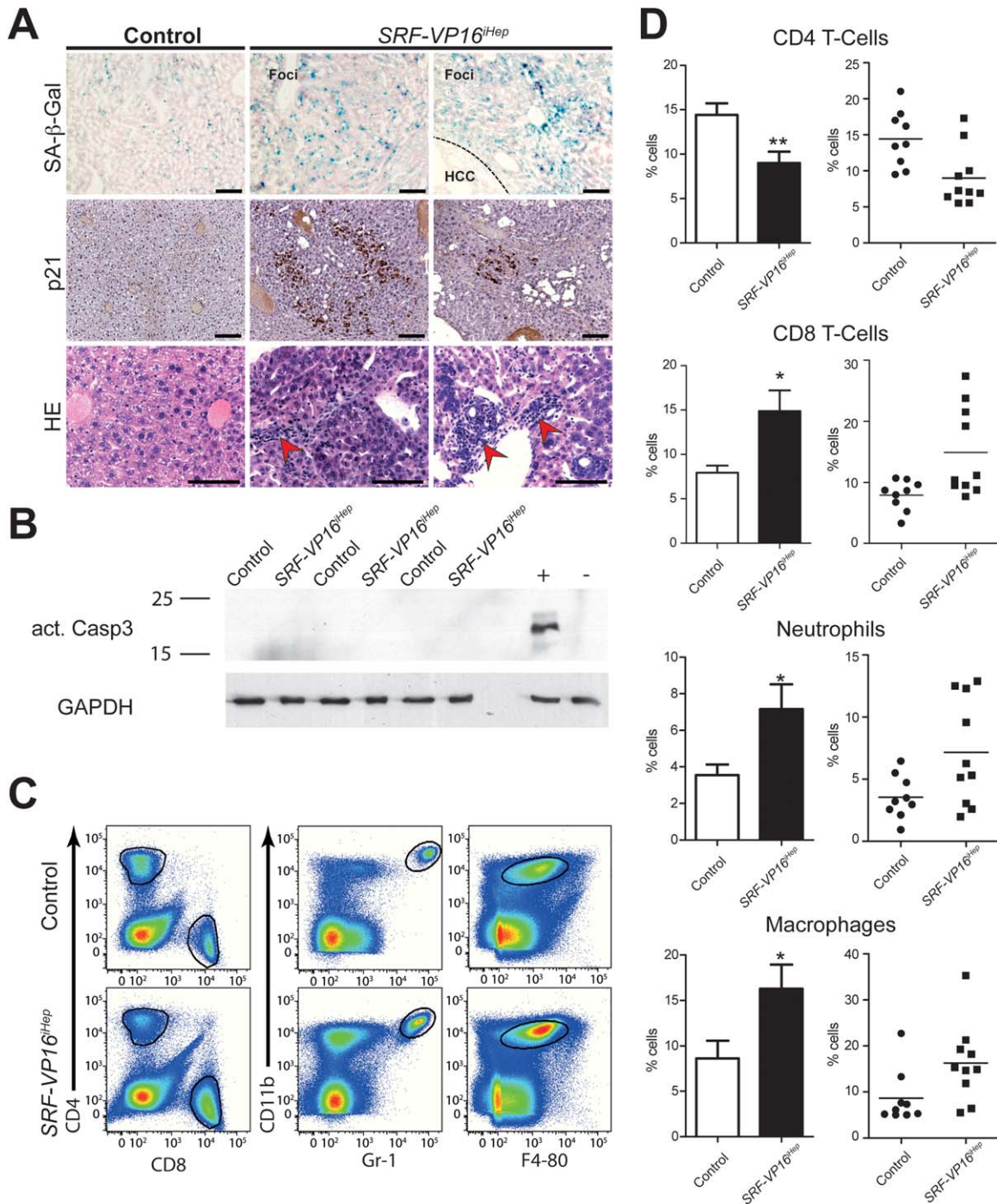
Fig. 4. Premalignant nodules harbor senescent hepatocytes and infiltrating lymphocytes. (A) Senescent hepatocytes in premalignant nodules of *SRF-VP16*[iHep] mice express SA-β-galactosidase (upper) and p21 (middle), and display foci of infiltrating immune cells (red arrowheads, lower). No β-bal signal is seen in HCC (upper, right). Scale bar = 100 μm. (B) Western blotting of activated Caspase 3, including positive (+) and negative (−) protein controls. (C,D) Immunophenotyping (flow cytometry) identifies neutrophil (CD11b^{high}Gr-1^{+}) infiltration into nodular livers, macrophages (CD11b^{+}F4/80^{+}), and CD8^{+} T cells, while CD4^{+} T cells are decreased. *$P < 0.05$ and **$P < 0.01$. Values represent mean ± SEM.

transcripts were found differentially expressed in nodular and HCC tissues (Table S2). RT-PCR validation was obtained for all genes investigated (including those studied in Fig. 5, plus eight others). Many genes carrying identified CArG-boxes were up-regulated (e.g.,

Bcl-2, Ctgf, Egr1, Egr2, Flna, c-fos, Myh9, Tagln2, Tgfb2, Thbs1, Tpm1, Tuft1, Vcl1, Vim, Vil1, and *Zyx*).[27] The Venn diagram (Fig. 6a) revealed 224 dysregulated transcripts shared by all three types of liver tissue (Category I, Table S3) and a distinct set of 358

		Srf genotype	SRF-VP16	Alfp-CreER[T2]	Age (weeks)	LBWR	SRF-VP16	Dusp2	Egr1	Egr2	Fos	Actb	Vcl	Ctnnb1	Myc	Cdh1	Mmp14	Vim	Car3	Cyr61	Cdk16	Snai1
								i — IEG / MAPK				**ii — Actin dyn.**		**iii — HCC prolif.**		**iv — HCC progression**			**v — other**			
controls	C1	f/f	-	-	33.9	4.5%	0.0	2.9	0.1	0.7	1.1	0.6	0.9	1.0	2.7	0.4	1.9	2.5	0.3	0.8	0.9	1.6
	C2	f/f	-	-	17.7	4.5%	0.0	0.8	0.4	1.3	0.6	1.0	0.8	0.8	0.5	0.8	0.7	0.6	1.5	0.8	1.0	1.3
	C3	f/f	-	-	17.6	4.5%	0.0	0.4	0.6	0.3	0.5	0.7	0.8	0.8	0.3	0.7	0.6	0.4	0.6	0.9	0.9	0.6
	C4	f/f	+	-	17.7	4.8%	0.0	0.6	1.1	0.2	1.5	0.8	1.3	0.9	2.7	1.2	0.9	0.9	0.6	0.7	0.9	0.5
	C5	f/f	-	-	17.6	5.0%	0.0	0.5	3.7	1.3	0.6	1.4	1.5	1.6	1.3	1.9	0.8	0.7	2.0	1.0	1.3	0.7
	C6	f/f	-	-	14.9	5.0%	0.0	1.5	1.4	3.4	2.8	2.0	0.9	0.8	0.2	0.8	1.4	1.1	2.0	0.9	0.9	1.4
	C7	f/f	-	-	17.6	5.0%	0.0	0.4	0.2	0.3	0.5	0.8	1.4	1.1	0.2	0.8	0.8	0.6	0.7	1.6	1.1	0.7
	C8	f/wt	-	+	12.4	5.2%	0.0	0.5	0.9	0.6	0.7	1.0	0.7	1.0	0.4	1.7	0.9	1.3	0.5	1.3	1.1	1.6
	C9	f/f	+	-	14.9	5.3%	0.0	1.3	0.4	0.8	0.7	0.7	0.6	1.0	0.7	0.8	1.4	0.8	0.7	1.0	0.9	1.6
premalignant nodules	N!	f/f	+	+	14.9	6.6%	0.2	0.8	5.2	26.3	7.7	1.2	1.0	1.0	0.2	1.4	1.5	0.9	1.0	0.6	0.9	1.4
	N1	f/f	+	+	17.6	7.7%	0.5	2.0	14.3	37.2	8.8	1.3	2.5	1.0	0.8	5.8	1.2	1.6	1.2	1.4	1.2	0.6
	N3	f/f	+	+	25.1	9.6%	0.3	1.2	9.5	84.1	22.9	1.9	3.4	2.5	0.7	7.1	0.4	1.8	0.5	0.2	0.3	0.3
	N4	f/f	+	+	17.6	10.5%	0.4	1.1	11.5	78.1	11.1	1.7	2.5	0.9	0.5	6.3	1.7	1.2	0.8	0.8	1.1	1.3
	N5	f/f	+	+	34.1	15.4%	0.7	6.6	17.4	180.2	43.1	1.8	4.1	0.9	1.3	8.8	3.0	3.7	0.0	1.9	1.4	1.6
	N6	f/f	+	+	23.0	15.7%	0.5	5.0	7.0	133.2	17.0	1.6	2.6	1.7	1.9	7.1	1.9	1.3	0.0	0.7	0.8	1.3
	N7	f/wt	+	+	17.7	15.7%	1.0	1.8	14.2	8.5	12.0	1.4	1.3	1.2	0.9	6.7	1.4	3.1	0.1	0.6	1.0	0.6
	N8	f/wt	+	+	17.7	15.9%	3.1	8.8	33.3	80.4	43.2	3.3	2.3	2.0	1.1	6.5	8.0	3.3	0.0	0.8	1.1	2.9
	N9	f/wt	+	+	17.7	16.6%	1.5	1.9	33.0	255.0	71.0	2.2	4.2	1.8	2.3	10.5	1.7	6.6	0.5	2.3	1.0	1.4
	N10	f/f	+	+	21.6	17.8%	0.7	1.8	25.2	38.7	12.8	0.9	2.1	1.2	1.4	6.1	1.8	2.9	0.5	0.9	1.1	1.5
	N11	f/wt	+	+	21.6	17.8%	1.3	2.6	15.6	42.3	10.2	3.1	2.4	1.7	1.0	7.1	2.1	2.7	0.3	1.6	1.4	1.0
	N12	f/wt	+	+	21.6	19.4%	1.0	5.2	14.0	33.0	8.1	1.5	2.6	2.2	2.2	9.4	4.4	5.4	0.1	1.1	1.1	2.3
	N13	f/f	+	+	30.7	20.1%	2.2	9.2	30.6	304.7	39.3	2.4	3.1	1.7	1.3	7.9	5.2	4.3	0.0	1.8	1.5	2.3
	N14	f/f	+	+	23.7	21.5%	0.8	1.0	14.0	222.2	55.9	1.5	4.4	2.4	1.4	11.4	5.3	3.0	0.1	1.5	1.0	3.9
	N15	f/f	+	+	26.6	23.3%	0.9	2.7	17.0	147.1	36.3	1.4	4.1	2.8	2.3	10.1	3.5	4.7	0.1	1.1	0.9	1.3
	N16	f/f	+	+	20.3	26.6%	0.4	1.8	9.0	86.3	26.8	1.1	2.3	1.8	0.8	6.0	4.6	2.2	0.1	1.1	0.8	3.9
	N17	f/f	+	+	26.3	26.9%	0.9	1.4	11.9	183.0	23.4	1.2	3.5	2.0	1.2	9.3	4.4	3.9	0.1	0.8	1.0	2.2
HCC	H1	f/wt	+	+	36.0	21.4%	3.8	1.3	30.8	45.7	29.3	4.3	7.8	5.0	3.6	17.0	6.2	26.7	0.0	1.5	1.7	1.8
	H2*	f/wt	+	+	30.0	25.3%	3.4	1.7	23.2	56.2	31.8	3.6	13.4	38.6	7.1	10.5	12.5	58.7	0.2	2.4	3.8	2.6
	H3*	f/f	+	+	31.9	24.3%	4.9	3.7	50.6	203.0	20.0	8.2	13.6	8.5	3.6	24.4	5.5	56.6	0.0	1.0	2.9	4.0
	H4*	f/wt	+	+	30.0	25.3%	3.5	1.6	25.6	40.4	36.3	3.9	6.8	23.3	4.4	15.4	7.8	27.5	0.2	2.2	1.9	1.5
	H5*	f/f	+	+	20.3	26.6%	2.2	3.2	21.9	100.3	8.5	2.2	8.7	2.3	2.0	19.7	10.5	11.4	0.1	0.5	1.8	1.7

fold change legend: ≤ 0.1 | 0.2 | 0.5 | 1.0 | 2.0 | 5.0 | ≥ 10

Fold mean difference nodule vs. control:

Dusp2	Egr1	Egr2	Fos	Actb	Vcl	Ctnnb1	Myc	Cdh1	Mmp14	Vim	Car3	Cyr61	Cdk16	Snai1
3.2	16.6	114.1	29.7	1.7	2.8	1.7	1.2	7.5	3.1	3.1	0.3	1.1	1.0	1.8
*	***	***	**	**	***	**	n.s.	***	**	***	**	n.s.	n.s.	*

Fold mean difference HCC vs. control:

Dusp2	Egr1	Egr2	Fos	Actb	Vcl	Ctnnb1	Myc	Cdh1	Mmp14	Vim	Car3	Cyr61	Cdk16	Snai1
2.3	30.4	89.1	25.2	4.4	10.1	15.6	4.1	17.4	8.5	36.2	0.1	1.5	2.4	2.3
n.s.	**	**	*	**	**	n.s.	*	**	**	**	n.s.	*	*	*

Fold mean difference HCC vs. nodule:

Dusp2	Egr1	Egr2	Fos	Actb	Vcl	Ctnnb1	Myc	Cdh1	Mmp14	Vim	Car3	Cyr61	Cdk16	Snai1
0.7	1.8	0.8	0.8	2.6	3.5	9.2	3.3	2.3	2.8	11.7	0.4	1.4	2.3	1.3
n.s.	n.s.	n.s.	n.s.	n.s.	**	n.s.	*	*	*	*	n.s.	n.s.	*	n.s.

Fig. 5. SRF-VP16[iHep] liver tissues display altered gene expression profiles. Expression of candidate genes in liver tissue of control mice (C1-C9), and premalignant nodular tissue (F1-F17) and mHCCs (H1-H5) of SRF-VP16[iHep] mice. Genotype abbreviations: f, Srf-flex1; wt, wild-type; SRF-VP16 +, positive; SRF-VP16 –, negative; Alfp-CreER[T2] +, positive; Alfp-CreER[T2] –, negative). Functional grouping of candidate genes and relative expression levels (q-RT-PCR) (numerical and by heat-map coloring) is indicated. Tissue samples are arranged by increasing LBWR (%), tumors by size (H1 and H2: 1.0 cm, H3: 2.0 cm, H3-H5: 2.5 cm).

transcripts dysregulated in HCCs but not nodules (Category II, Table S4). In all, 68 (Category III, Table S5), 226 (Category IV, Table S6) and 317 transcripts (Category V, Table S7) were dysregulated exclusively in nodular tissue, mHCC_A, and mHCC_B, respectively. For each category, the 10 most strongly up- and down-regulated genes are displayed (Fig. 6B). The 25 most strongly up-regulated transcripts of Categories I and II represented oncofetal genes (Igf2, H19, Bex1), and genes involved in proliferation/survival (Cpe, Gldn, Fstl3, Psat1, Igf2, Cd63, Lcn2, Plat1, Tspan8, Tspan13, Timp1), cytoskeletal activities (Actn3, Krt20, Vim, Vil1), immune-regulation (Ly6d, Klrb1a) and lipid metabolism (Scd2, Ly6d, Akr1c18, Lpl2). The Ctnnb1-mutated HCC_B tumors (Category V) selectively showed up-regulation of proto-oncogenes c-fos, and c-Jun, as well as Wnt signaling components (Fzd3, Lef1, Tcf7, Axin2). Down-regulated transcripts of Categories I and II included the tumor suppressor genes Sdha, Ndrg2 and Igfals.[22,28]

Shared Gene Expression Signatures of Murine and hHCCs. Cross-species comparison of our murine samples was performed with a cohort of 40 human HCCs,[22] which was analyzed for genomic DLC1 deletions, SRF mRNA expression, and CTNNB1 mutation status (Fig. 6C). 60% hHCCs displayed genomic DLC1 loss and 50% displayed SRF mRNA overexpression (Fig. 6C). Tumors overexpressing SRF either displayed elevated IGF2 expression or clustered with CTNNB1 mutations (Fig. 6C,D, upper). Further, hHCC subclasses (G1 to G6) were assigned according to Boyault classification.[2] Combined unsupervised hierarchical clustering of gene expression profiles from murine and hHCCs was performed, applying a gene set of the SRF-VP16-derived "58 most strongly up-regulated transcripts." A strong murine/human expression overlap with a subgroup of 10 hHCCs, henceforth called "subcluster of 10" (SC10), was observed (Fig. 6D). SC10 hHCCs displayed a stronger relatedness to the murine specimen than to any of the other 30
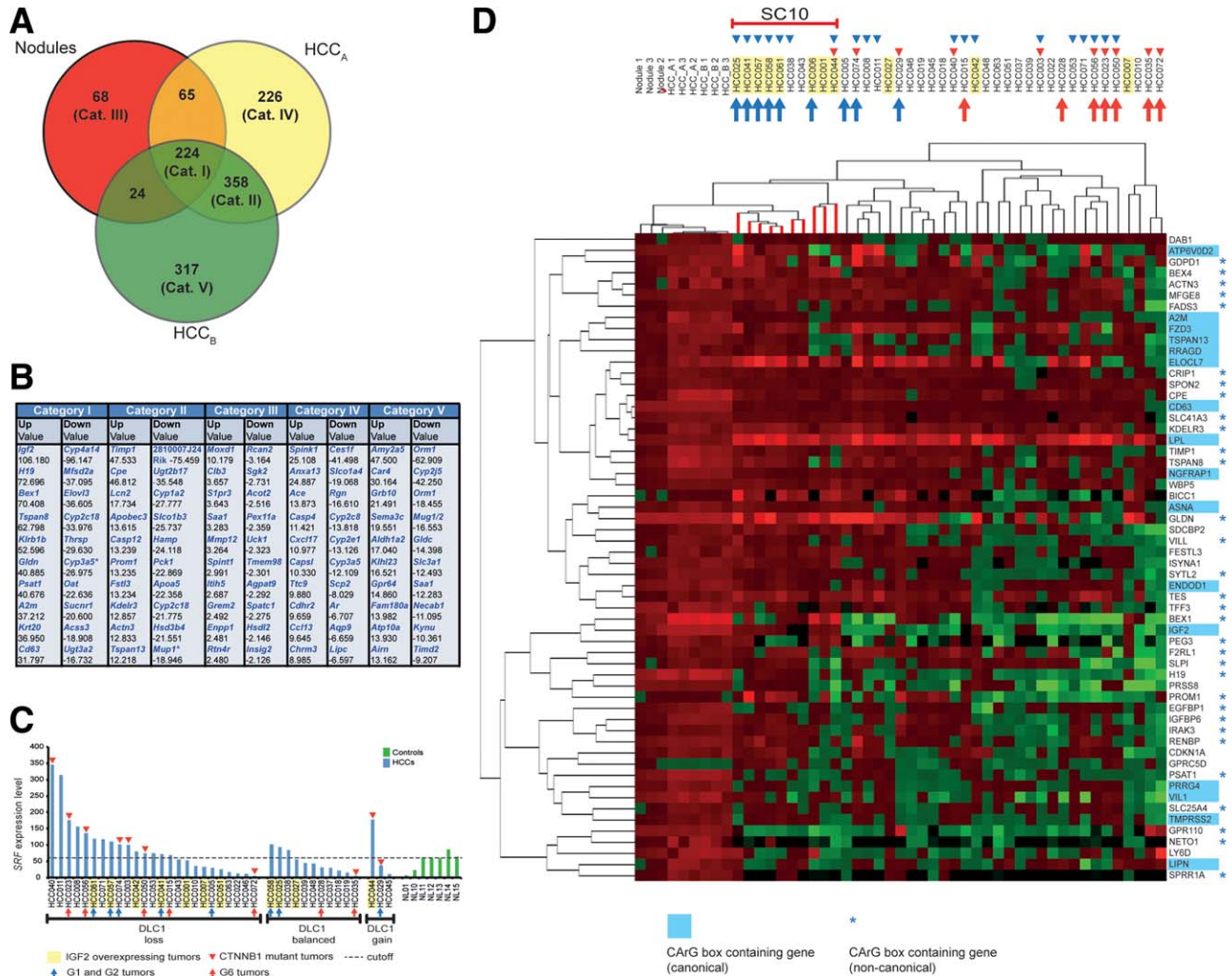
Fig. 6. SRF-VP16-triggered mHCCs share expression profiles with G1/G2 subgroups of hHCCs. (A) Venn diagram depicting differentially expressed transcripts in all three types of tissue (Category I), mHCCs (Category II), nodular tissue (Category III), mHCCs without *Ctnnb1* mutation (HCC_A; Category IV), and mHCCs with *Ctnnb1* mutation (HCC_B; Category V). (B) Listing of 10 most strongly up- or down-regulated transcripts per category (x-fold differential expression). (C) Cohort of 40 hHCCs grouped according to genomic *DLC1* status (x-axis) and *SRF* mRNA expression levels (Y-axis). *IGF2* RNA overexpression status (yellow box), *CTNNB1* mutation status (red triangle), Boyault class (G1 and G2, blue arrow; G6, red arrow). (D) Combined unsupervised hierarchical clustering of the 58 most strongly up-regulated transcripts in SRF-VP16-triggered nodular/mHCC tissue against 40-membered hHCC cohort (blue triangles: SRF overexpressing tumors, other symbols as in (C)). The "subcluster of 10" hHCCs (SC10) cluster close to the mHCCs. Murine genes contain a canonical (blue box) or noncanonical CArG-box (blue asterisks).

hHCCs and were enriched for *IGF2*-overexpressing tumors. 70% of the G1 or G2 tumors belonged to SC10, while none of the G6 tumors did (Fig. 6D). In close agreement, upon applying the murine gene set of "50 most dysregulated (up or down) transcripts in the unsupervised hierarchical clustering," a subcluster of eight human tumors (SC8) was identified (not shown). All tumors of SC8 are contained in SC10. Individual genes specifying the mHCC/hHCC overlap included the imprinted or developmentally expressed genes *Igf2*, *H19*, *Bex1, Peg3*, and *Cd133/Prom1*. Additional development-regulated transcripts dysregulated in SRF-VP16 tissues included oncofetal genes *Afp, Epcam, Gpc3, Igf2bp3, Plaur, Sox4, Sox9, Vil1,* and *Vim*. In summary, comparative expression profiling identified high relatedness between SRF-VP16-derived mHCCs and hHCCs, particularly the G1/G2-enriched SC10 subset. The commonality included dysregulation of oncofetal gene expression.

Epigenetic Dysregulation of** Igf2/H19 **in Both Murine and Human HCCs. Overexpression of the normally imprinted *Igf2/H19* genes in both SRF-VP16-derived mHCCs (Fig. 7A) and G1 subclass hHCC[2] suggested common epigenetic alterations. CpG methylation of the *Igf2/H19* imprinting control region (*DMR*), investigated in 40 independent SRF-VP16-triggered mHCCs, indeed revealed hypomethylation in both nodules and tumors (Fig. 7B), correlating with
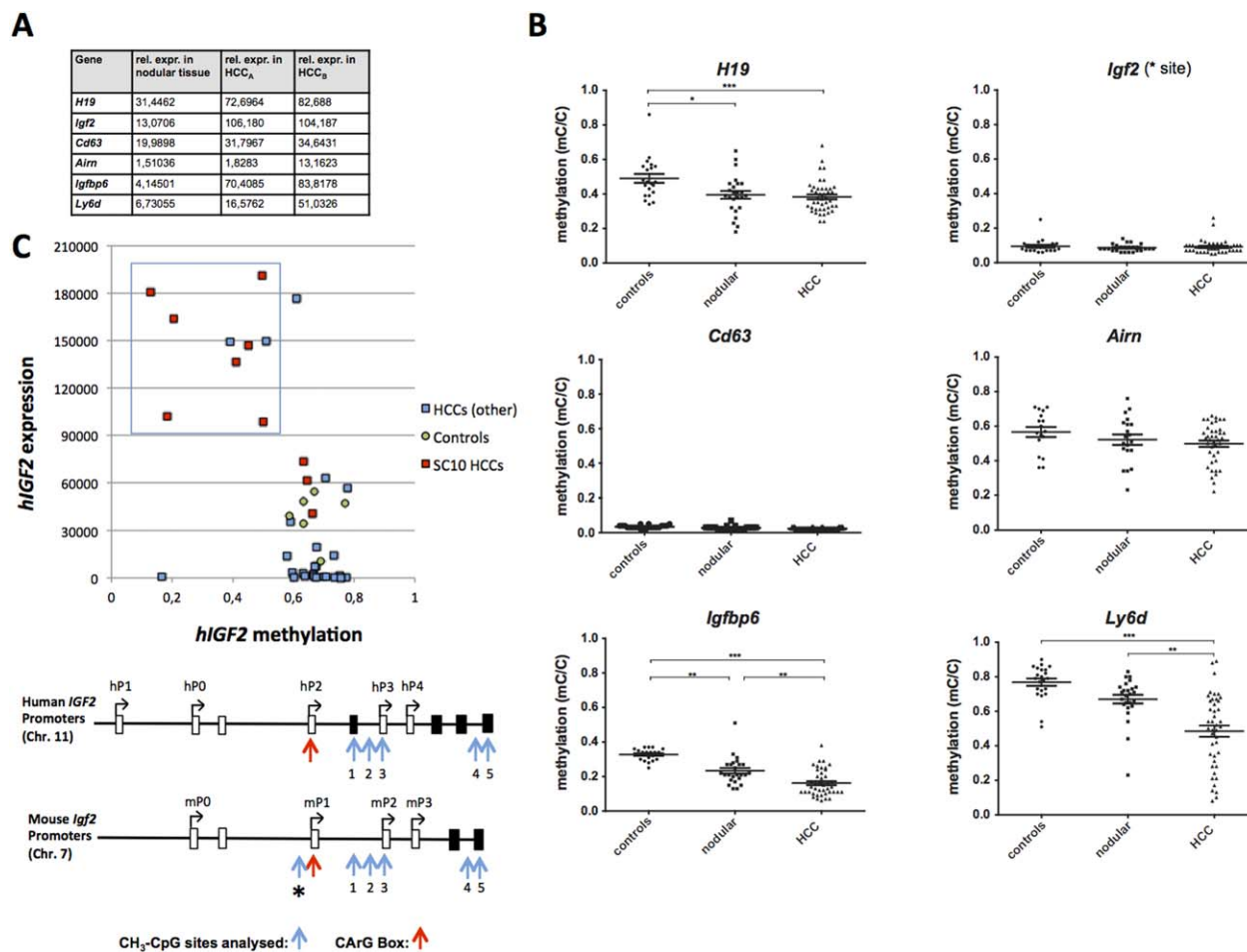
Fig. 7. Genomic methylation profiles of selected sites in murine and human HCCs. (A) Selected transcript expression in *SRF-VP16*[iHep] mice. (B) Genomic CpG methylation ratios (mC/C) at the indicated gene loci of murine tissues. *H19* locus investigated at imprinting control region (*Igf2/H19 DMR*), other genes investigated at promoter. (C) 40-membered hHCC cohort: averaged methylation ratio of CpG sites 1-3 of human *IGF2* hP3 promoter blotted versus corresponding *hIGF2* mRNA expression levels. Boxed: hHCC subgroup with reduced CpG methylation and concomitantly elevated *IGF2* expression. Lower: 5′ regions of the human *IGF2* gene (hP0 to hP4 promoters) and the murine *Igf2* gene (mP0 to mP3 promoters).

elevated *H19* gene expression. Regarding the highly expressed *Igf2* gene in murine HCCs, no differences to constitutive low control levels of CpG methylation were seen upstream of the mP1 promoter (site *, Fig. 7B) nor around the mP2 promoter (sites 1-3, Fig. S3), similar to the highly expressed *Cd63* gene (Fig. 7B). Promoter-associated CpG sites of the imprinted *Airn* gene, encoding an antisense regulator of *Igf2r*, showed a trend towards demethylation, which might be hyperproliferation-associated, but this failed to reach statistical significance. Also, the *Meg3* and *Peg3* genes, usually subject to imprinting control, were strongly overexpressed in SRF-VP16-triggered mHCC (Table S3). Other highly expressed genes, *Igfbp6* and *Ly6d*, displayed significant CpG hypomethylation (Fig. 7B). Collectively, this indicates SRF-VP16-triggered mHCC formation being linked to epigenetic alterations of both imprinted and nonimprinted genes.

Since elevated *hIGF2* expression is frequent in human G1-type HCCs,[2] we investigated the cohort of 40 human HCCs regarding *hIGF2* expression and CpG methylation. We focused on three CpG dinucleotides around the hP3 promoter (sites 1-3; Fig. 7C, lower), previously implicated in tumor-associated hP3 promoter activation.[29] 25% of hHCC specimens, including the majority of G1/G2 tumors and the SC10 tumors, showed both high *hIGF2* gene expression and promoter hP3 hypomethylation (Fig. 7C, upper). Thus, the SC10 subtype of hHCC display *hIGF2* promoter hypomethylation congruent with SRF-VP16-triggered mHCC.

Discussion

SRF-VP16[iHep] mice provide the first *in vivo* evidence for dysregulated, constitutive activity of the transcription factor SRF to trigger cancer. Constitutive SRF-VP16

activity elicited gene expression profiles, which mirrored, in part, SRF activity stimulated by combined Ras/MAPK and Rho/actin signaling (Fig. 1A),[13,14] pathways frequently activated in cancer cells.[6,12] A comparable scenario was revealed for oncogenic human Ets proteins in mimicking Ras/MAPK signaling.[30]

In *SRF-VP16*[iHep] mice, within 10 weeks, spontaneous hepatocellular activation of CreER[T2] generated an SRF-VP16-overexpressing cell population constituting ~0.4% of all hepatocytes. The single molecular event of induced SRF-VP16 expression elicited high proliferative activity, leading to rapid hepatocyte expansion and formation of premalignant dysplastic lesions (nodules). Subsequently, from these numerous nodules progression to a small number of malignant HCC occurred. The *SRF-VP16*[iHep] mouse model therefore permits the study of molecular events associated with both initiation and progression of cancer. Close to 50% of murine SRF-VP16-triggered tumors displayed activating point mutations in the *Ctnnb1* gene, mapping to codons equivalent to those mutated in hHCCs.

The profile of dysregulated genes in *SRF-VP16*[iHep] mHCCs encompasses a subgroup of 182 entries shared with the 960-membered set of direct SRF target genes mediating the serum response of transformed fibroblasts[27] (Table S8). This strong overlap attests to SRF-VP16 indeed impacting efficiently CArG-box containing genes in hepatocytes of *SRF-VP16*[iHep] mice. Elevated expression of the IEGs *Egr1, Egr2*, and c-*fos*, well-known proliferation-associated SRF target genes,[31] was seen at the onset of nodule formation (at 6.6% LWBR) (Fig. 5). Nodular activation of *Igf2* likely also contributed to SRF-VP16-mediated hepatocellular expansion, and overexpression of *IGF2* has long been known to contribute to HCC formation.[2,32]

Expression profiles of SRF-VP16-triggered mHCCs revealed striking overlap with Boyault classified G1 and G2 subclasses of hHCC.[2] This molecular resemblance rested on overlap regarding the subset of 58 most strongly overexpressed genes in mHCCs, which included oncofetal genes. Oncofetal/developmental genes were also strongly overexpressed in the HB hepatoblast-like subtype of hHCC,[33] sharing characteristics with G1 hHCCs. The expression overlap between SRF-VP16-triggered mHCCs and hHCCs suggests that, in human cancer patients, hyperactivated SRF contributes to HCC formation of G1/G2 (and HB) subtypes. Consistently, the cohort of 40 hHCCs analyzed here shows enrichment of G1/G2 tumors among the hHCC subset displaying elevated *SRF* expression (Fig. 6C,D).

Molecular congruence between SRF-VP16-elicited mHCCs and G1/G2 hHCCs was also found regarding loss of imprinting and dysregulation of promoter CpG methylation. Based on the analysis of 40 SRF-VP16-triggered mHCCs, loss of CpG methylation at the *DMR* of the imprinted *Igf2/H19* locus was observed (Fig. 7B), as similarly reported for G1 subtype hHCCs.[2] Furthermore, the hHCC cohort studied here revealed CpG hypomethylation at the human *IGF2* hP3 promoter in the majority of SC10/(G1/G2) hHCCs. This correlated with elevated *hIGF2* expression (Fig. 7C) and reflected the constitutively low CpG methylation at *mIgf2* promoters in murine tissues (Fig. S3). Yet the precise mechanism leading to the massive deregulation of the *Igf2/H19* locus in the SRF-VP16-triggered mHCCs remains to be elucidated.

Within an individual *SRF-VP16*[iHep] liver, only few isolated mHCC lesions develop from thousands of premalignant nodules (Fig. 1), indicating tumor suppressor mechanisms preventing malignant transformation to occur more frequently. The presence of senescent hepatocytes within and surrounding the premalignant nodules, plus the presence of infiltrating leukocytes (Fig. 4), suggested tumor suppression by senescence-associated immune surveillance[26,34] to govern the mouse model.

In conclusion, the *SRF-VP16*[iHep] mouse model, which is shown to display, in part, gene expression profiles elicited upon combined oncogenic Ras/MAPK and Rho/actin signaling, identifies SRF target genes to fulfill oncogenic driver functions in HCC. SRF activation by virally expressed HBV and HCV proteins[17] adds a clinically relevant component to SRF's suggested role in liver carcinogenesis. The molecular relationship between SRF-VP16-triggered mHCCs and G1/G2 hHCCs strengthens our suggestion of SRF playing a crucial role in liver carcinogenesis. Simultaneous molecular targeting of both Ras/MAPK and Rho/actin signaling pathways, including direct inhibition of SRF, is suggested as a therapeutic strategy for treatment of human HCC.

References

1. Jemal A, Bray F, Center MM, Ferlay J, Ward E, Forman D. Global cancer statistics. CA Cancer J Clin 2011;61:69-90.
2. **Boyault S, Rickman DS, de Reynies A**, Balabaud C, Rebouissou S, Jeannot E, et al. Transcriptome classification of HCC is related to gene alterations and to new therapeutic targets. HEPATOLOGY 2007;45:42-52.

3. **Guichard C, Amaddeo G, Imbeaud S**, Ladeiro Y, Pelletier L, Maad IB, et al. Integrated analysis of somatic mutations and focal copy-number changes identifies key genes and pathways in hepatocellular carcinoma. Nat Genet 2012;44:694-698.

4. Hoshida Y, Nijman SM, Kobayashi M, Chan JA, Brunet JP, Chiang DY, et al. Integrative transcriptome analysis reveals common molecular subclasses of human hepatocellular carcinoma. Cancer Res 2009;69: 7385-7392.

5. Calvisi DF, Ladu S, Gorden A, Farina M, Conner EA, Lee JS, et al. Ubiquitous activation of Ras and Jak/Stat pathways in human HCC. Gastroenterology 2006;130:1117-1128.

6. Whittaker S, Marais R, Zhu AX. The role of signaling pathways in the development and treatment of hepatocellular carcinoma. Oncogene 2010;29:4989-5005.

7. Xue W, Krasnitz A, Lucito R, Sordella R, Vanaelst L, Cordon-Cardo C, et al. DLC1 is a chromosome 8p tumor suppressor whose loss promotes hepatocellular carcinoma. Genes Dev 2008;22:1439-1444.

8. Lahoz A, Hall A. DLC1: a significant GAP in the cancer genome. Genes Dev 2008;22:1724-1730.

9. Sahai E, Marshall CJ. RHO-GTPases and cancer. Nat Rev Cancer 2002;2:133-142.

10. Durkin ME, Yuan BZ, Zhou X, Zimonjic DB, Lowy DR, Thorgeirsson SS, et al. DLC-1:a Rho GTPase-activating protein and tumour suppressor. J Cell Mol Med 2007;11:1185-1207.

11. Sahai E, Olson MF, Marshall CJ. Cross-talk between Ras and Rho signalling pathways in transformation favours proliferation and increased motility. EMBO J 2001;20:755-766.

12. Xia M, Land H. Tumor suppressor p53 restricts Ras stimulation of RhoA and cancer cell motility. Nat Struct Mol Biol 2007;14:215-223.

13. Olson EN, Nordheim A. Linking actin dynamics and gene transcription to drive cellular motile functions. Nat Rev Mol Cell Biol 2010;11: 353-365.

14. Posern G, Treisman R. Actin' together: serum response factor, its cofactors and the link to signal transduction. Trends Cell Biol 2006;16:588-596.

15. **Bai S, Nasser MW, Wang B**, Hsu SH, Datta J, Kutay H, et al. MicroRNA-122 inhibits tumorigenic properties of hepatocellular carcinoma cells and sensitizes these cells to sorafenib. J Biol Chem 2009;284: 32015-32027.

16. Park MY, Kim KR, Park HS, Park BH, Choi HN, Jang KY, et al. Expression of the serum response factor in hepatocellular carcinoma: implications for epithelial-mesenchymal transition. Int J Oncol 2007; 31:1309-1315.

17. Kato N, Yoshida H, Ono-Nita SK, Kato J, Goto T, Otsuka M, et al. Activation of intracellular signaling by hepatitis B and C viruses: C-viral core is the most potent signal inducer. HEPATOLOGY 2000;32:405-412.

18. Muehlich S, Hampl V, Khalid S, Singer S, Frank N, Breuhahn K, et al. The transcriptional coactivators megakaryoblastic leukemia 1/2 mediate the effects of loss of the tumor suppressor deleted in liver cancer 1. Oncogene 2012;31:3913-3923.

19. Hampl V, Martin C, Aigner A, Hoebel S, Singer S, Frank N, et al. Depletion of the transcriptional coactivators megakaryoblastic leukaemia 1 and 2 abolishes hepatocellular carcinoma xenograft growth by inducing oncogene-induced senescence. EMBO Mol Med 2013;5:1367-1382.

20. Sandstrom J, Heiduschka P, Beck SC, Philippar U, Seeliger MW, Schraermeyer U, et al. Degeneration of the mouse retina upon dysregulated activity of serum response factor. Mol Vis 2011;17:1110-1127.

21. Schratt G, Weinhold B, Lundberg AS, Schuck S, Berger J, Schwarz H, et al. Serum response factor is required for immediate-early gene activation yet is dispensable for proliferation of embryonic stem cells. Mol Cell Biol 2001;21:2933-2943.

22. Neumann O, Kesselmeier M, Geffers R, Pellegrino R, Radlwimmer B, Hoffmann K, et al. Methylome analysis and integrative profiling of human HCCs identify novel protumorigenic factors. HEPATOLOGY 2012;56:1817-1827.

23. Bamford S, Dawson E, Forbes S, Clements J, Pettett R, Dogan A, et al. The COSMIC (Catalogue of Somatic Mutations in Cancer) database and website. Br J Cancer 2004;91:355-358.

24. Wiebel FF, Rennekampff V, Vintersten K, Nordheim A. Generation of mice carrying conditional knockout alleles for the transcription factor SRF. Genesis 2002;32:124-126.

25. Stecca BA, Nardo B, Chieco P, Mazziotti A, Bolondi L, Cavallari A. Aberrant dipeptidyl peptidase IV (DPP IV/CD26) expression in human hepatocellular carcinoma. J Hepatol 1997;27:337-345.

26. Kang TW, Yevsa T, Woller N, Hoenicke L, Wuestefeld T, Dauch D, et al. Senescence surveillance of pre-malignant hepatocytes limits liver cancer development. Nature 2011;479:547-551.

27. Esnault C, Stewart A, Gualdrini F, East P, Horswell S, Matthews N, et al. Rho-actin signaling to the MRTF coactivators dominates the immediate transcriptional response to serum in fibroblasts. Genes Dev 2014;28:943-958.

28. **Marquardt JU, Seo D, Andersen JB**, Gillen MC, Kim MS, Conner EA, et al. Sequential transcriptome analysis of human liver cancer indicates late stage acquisition of malignant traits. J Hepatol 2014;60:346-353.

29. **Silviera ML, Smith BP**, Powell J, Sapienza C. Epigenetic differences in normal colon mucosa of cancer patients suggest altered dietary metabolic pathways. Cancer Prev Res (Phila) 2012;5:374-384.

30. Hollenhorst PC, Ferris MW, Hull MA, Chae H, Kim S, Graves BJ. Oncogenic ETS proteins mimic activated RAS/MAPK signaling in prostate cells. Genes Dev 2011;25:2147-2157.

31. Pritchard MT, Malinak RN, Nagy LE. Early growth response (EGR)−1 is required for timely cell-cycle entry and progression in hepatocytes after acute carbon tetrachloride exposure in mice. Am J Physiol Gastrointest Liver Physiol 2011;300:G1124-1131.

32. Schirmacher P, Held WA, Yang D, Chisari FV, Rustum Y, Rogler CE. Reactivation of insulin-like growth factor II during hepatocarcinogenesis in transgenic mice suggests a role in malignant growth. Cancer Res 1992;52:2549-2556.

33. Lee JS, Heo J, Libbrecht L, Chu IS, Kaposi-Novak P, Calvisi DF, et al. A novel prognostic subtype of human hepatocellular carcinoma derived from hepatic progenitor cells. Nat Med 2006;12:410-416.

34. Guo X, Keyes WM, Papazoglu C, Zuber J, Li W, Lowe SW, et al. TAp63 induces senescence and suppresses tumorigenesis in vivo. Nat Cell Biol 2009;11:1451-1457.

Author names in bold designate shared co-first authorship.

Supporting Information

Additional Supporting Information may be found at onlinelibrary.wiley.com/doi/10.1002/hep.27539/suppinfo.